

## MULTI-CLASS REGULARIZATION PARAMETER LEARNING FOR GRAPH CUT IMAGE SEGMENTATION

Sema Candemir<sup>\*</sup>, Kannappan Palaniappan<sup>†</sup>, and Yusuf Sinan Akgul<sup>\*†</sup>

<sup>\*</sup> Lister Hill National Center for Biomedical Communications, U. S. National Library of Medicine,  
National Institutes of Health, Bethesda, MD, USA

<sup>†</sup>Department of Computer Science, University of Missouri-Columbia, MO, USA

<sup>\*†</sup> Department of Computer Engineering, Gebze Institute of Technology, Gebze, Turkey

### ABSTRACT

One of the first steps of computer-aided systems is robustly detect the anatomical boundaries. Literature has several successful energy minimization based algorithms which are applied to medical images. However, these algorithms depend on parameters which need to be tuned for a meaningful solution. One of the important parameters is the regularization parameter ( $\lambda$ ) which is generally estimated in an ad-hoc manner and is used for the whole data set. In this paper we claim that  $\lambda$  can be learned by local features which hold the regional characteristics of the image. We propose a  $\lambda$  estimation system which is modeled as a multi-class classification scheme. We demonstrate the performance of the approach within graph cut segmentation framework via qualitative results on chest x-rays. Experimental results indicate that predicted parameters produce better segmentation results.

### 1. INTRODUCTION

The chest films contain important information about the condition of the patients. However, their interpretation is not trivial which encourage the researchers to develop computer algorithms to assist the radiologist in diagnosis process. Automatic segmentation of anatomical fields is one of the first steps of such computer-aided systems. Some of the abnormalities and diagnostic information can be directly extracted from the anatomical boundaries such as Total Lung Capacity which aids in detection of pneumonia, pulmonary atelectasis or obstructive airways diseases [1]. Some algorithms need anatomical boundaries for the further stages such as tuberculosis classification [2]. Robust segmentation of anatomical shapes is needed in order to extract the diagnostic information accurately.

Literature have several energy minimization based approaches [3, 4] which are used to extract the anatomical boundaries. A common energy function for the segmentation task is,

$$E(f) = E_d(f) + \lambda E_s(f) \quad (1)$$

where  $f$  is the segmentation labels;  $E_d(f)$  is the data term and  $E_s(f)$  is the smoothness term. The data term confines the segmentation labels to be close to the observed image. The smoothness term forces the algorithm to assign similar labels to the neighborhood pixels. The smoothness term is included into the energy formulation with parameter  $\lambda$  which regularizes the smoothness degree of solution. Choosing a suitable  $\lambda$  is important to obtain a satisfactory segmentation [5]. If  $\lambda$  is small, the segmentation will be noisy. On the other hand, if  $\lambda$  is large, the segmentation will not fit the observed data.

Generally,  $\lambda$  is estimated in an ad-hoc manner and is used for the whole dataset. There are several regularization parameter estimation approaches, but are outside the scope of this paper because no image processing is involved. The regularization parameter depends on image statistics such as image noise and variation of scene structures [6, 7, 8]. Since images have different statistics,  $\lambda$  has to be estimated for each image separately for a better performance. This idea is illustrated on synthetic images in Figure 1. We minimize Eq 1 and plot the percentage error rate of segmentation versus regularization parameter  $\lambda$ . The minimum point of error- $\lambda$  curves (red point) is the optimal  $\lambda$  of each image. The graphs indicate that the optimal  $\lambda$  varies across different images for the same algorithm.

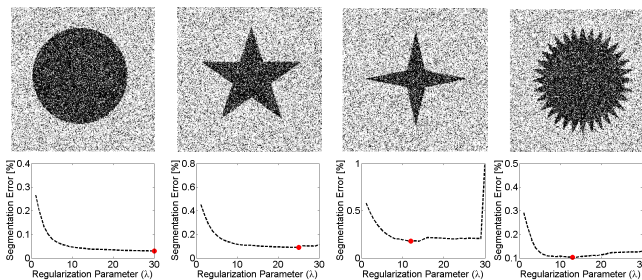


**Fig. 1.** The dependence of the energy functional (Eq 1) on parameter  $\lambda$  is shown for synthetic images which are corrupted by Gaussian white noise with standard deviation of 0.17. The error is the percentage of non-overlapping pixels between the segmentation and the ground truth.

Recently, it is accepted that a single  $\lambda$  is not optimal for all regions of the image especially on regions which have different image statistics. Therefore, spatially adaptive regularization has been acknowledged which modulate the effect of regularization in a heuristic manner using regional image cues. The proposed cues so far are image noise [9], gradient [10, 11], and curvature [12].

This paper proposes that regularization parameter of local regions can be learned using a classification algorithm by training with local feature vectors. We modeled the parameter estimation as a supervised classification scheme such that each region is assigned a regularization label according to the local statistics. The main contributions of the paper are (i) modeling the regularization parameter estimation as a multi-class classification scheme, and (ii) solving the regularization parameter estimation through a simple learning algorithm. To the best of our knowledge, the regularization parameter estimation through a classification framework was not attempted in the literature before.

We used multi-class boosting algorithm [13] for the classification scheme. We demonstrate the performance of our approach within graph cut segmentation [3, 4] due to its dependence on parameter  $\lambda$ . We show the qualitative results on a public lung database [14]. We describe the proposed system in Section 2 and give the experimental results in Section 3. The last section concludes the paper and discusses future work.

## 2. MULTI-CLASS REGULARIZATION LABELING

The multi-class regularization labeling system consist of three main stages: (i) The system first learns  $\lambda$  labels by training a boosting algorithm with local feature vectors of the training images. (ii) The trained system predicts a  $\lambda$ -map for the test image. (iii) An energy-based segmentation algorithm uses the predicted  $\lambda$ -map to segment the test image. Figure 3 illustrates the steps of the proposed system.

### 2.1. Learning and Estimating $\lambda$ Labels

System models the regional characteristics of x-rays using a set of shape and texture features. We used Haar based [15, 16] features to model edge and curvature information, local binary pattern [17] for texture information, and Hessian [18] for shape information. We then use the features to train the classifier. Let  $f_i^k$  denotes the  $k^{th}$  feature of  $i^{th}$  pixel of image  $I$ . The feature vector of pixel  $i$  is obtained by concatenating all features as  $f_i = [f_i^1, f_i^2, \dots, f_i^K]^T$ . Using the feature vectors  $f_i$ , we train a boosting algorithm and classify the feature vectors of a given image into one of the  $\lambda$  classes.

For the training stage, we define the corresponding  $\lambda_i$  label of feature vector  $f_i$  automatically with the help of the ground truth segmentation. The system assigns an arbitrary  $\lambda_i$  label for each pixel among the 10 class labels initially. Then,

it measures the segmentation error by assigning other labels in the set. The  $\lambda$  map with local minimum error is used as the ground truth label map for the training image. Experimental results in Section 3 validate the adequacy of the ground truth labels.

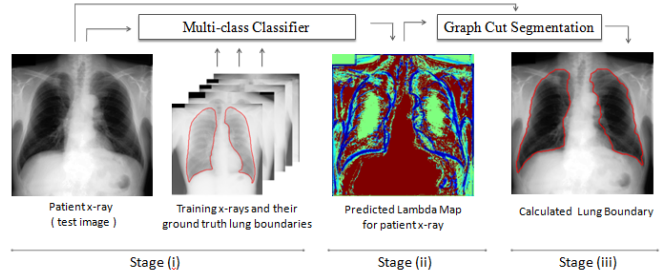


**Fig. 2.** The Framework of Multi-Class Regularization Labeling

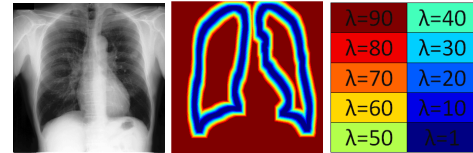


**Fig. 3.** The  $\lambda$ -map is shown in color map. Blue pixels indicate smaller  $\lambda$  labels, and data term will be more effective at these regions. Red pixels indicate larger  $\lambda$  labels, so smoothness term will be more effective at these regions.

We train the system using a multi-class boosting [13] algorithm with the feature set  $\{f_i, y_i\}_{i=1}^N$  where  $f_i$  is the feature vector,  $y_i \in \lambda$  is the regularization label of pixel  $i$ , and  $N$  is the number of pixels on the image. The learning algorithm starts with weak hypotheses and produces a more accurate classifier by iteratively refining and combining the weak learners. The trained system estimates  $\lambda$  labels of a test image per pixel base.

### 2.2. Segmentation with Predicted $\lambda$ Map

Predicted  $\lambda$  labels are used in graph-cut image segmentation framework. We formulate the objective function in Eq 1 as follows:

$$E(f) = \sum_{p \in P} \ln(\|I_p - I_S\| + \epsilon) + \sum_{p, q \in N} \lambda_p \exp(-(I_p - I_q)^2), \quad (2)$$

where  $I_p$  is the intensity at pixel  $p$ ,  $I_S$  is the object or background label intensity,  $N$  is the neighborhood pixels  $q$  around pixel  $p$ . Object and background label intensities are determined with random seeds (0.5% of image pixels for each label) using ground truth mask.  $\lambda$ -map is incorporated into the objective function in second term (smoothness term) with  $\lambda_p$  which represents the predicted  $\lambda$  for pixel  $p$ .

There are two points that distinguish our work from the literature. (i) Feature vectors model the image region characteristics better than a single local image cue. Thus, proposed algorithm estimates more reliable regularization parameters for the image. (ii) The supervised learning based structure of the approach makes it possible to incorporate additional features into the algorithm.

### 3. EXPERIMENTS

We evaluate the proposed system on a publicly available chest x-ray data set which is compiled by the Japanese Society of Radiological Technology (JSRT) [14]. The JSRT data set contains 247 chest x-rays, among which 154 x-rays have tuberculosis nodules and 93 x-rays are normal. The data set has ground truth segmentation masks [19]. We have chosen 5 random images from the data set for training. The remainder of the set is used for testing.

As quantitative measure, we use the overlap percentage of segmentation and ground truth boundaries as follows:

$$\Omega = \frac{TP}{TP + FP + FN} \quad (3)$$

where TP is true positive (area correctly classified as object), FP is false positive (area incorrectly classified as object), and FN is false negative (area incorrectly classified as background). We compare the predicted regularization labels against i) single-global  $\lambda$  for data set, ii) gradient-based spatially adaptive method [11], and iii) curvature-based spatially adaptive method [12]. Graph cut algorithm segments x-rays with calculated  $\lambda$  parameter. For fair comparison, we keep all other graph cut parameters equal for compared methods.

Computational time for feature extraction takes 64s, training takes 110s, estimating  $\lambda$  labels takes 22s, and graph cut segmentation takes 8s for a 1024x1024 x-ray on a computer with 2.27GHz Intel Core 2 Duo CPU and 3GB memory. Training stage is executed only one time. Boosting and graph cut optimization tasks are carried out in C++, and visualization part is implemented in Matlab.

**Single-Global Lambda for Data set:** Generally  $\lambda$  is estimated in an ad-hoc manner and is used for the whole data set. We calculated a global  $\lambda$  ( $\lambda_G$ ) for 15 test images from data set by trial and error approach. The  $\lambda$  which produces minimum segmentation error ( $1-\Omega$ ) for the subset is defined as global  $\lambda$ .

**Spatially Adaptive Methods:** We compared the proposed method with spatially adaptive methods which uses gradient [11] and curvature [12] cues of image regions. In the experiments, we first calculate these features. Then, we adaptively change the  $\lambda$  according to the local cue information.

**Ground Truth  $\lambda$  Map:** The segmentation performance of the proposed method depends on two modules of the system: (i) feature extraction, and (ii) region classification for  $\lambda$  labeling. If feature extraction and classification are done successfully, the system estimates better  $\lambda$  for regions. In order to show that better predicted  $\lambda$  map produces better seg-

mentation, we segment the images with ground truth  $\lambda$  maps. Segmentation with ground truth  $\lambda$ -maps also validate the adequacy of ground truth labels.

In the experiments, single-global  $\lambda$ , adaptive  $\lambda$  with curvature cue, adaptive  $\lambda$  with edge cue, ground truth  $\lambda$ -map and predicted  $\lambda$ -map are labeled as  $\lambda_G$ ,  $\lambda_C$ ,  $\lambda_E$ ,  $\lambda_{GT}$  and  $\lambda_P$ , respectively. Figure 4 shows the graph cut segmentation with  $\lambda$ -maps on chest x-rays. The overlap scores of all segmentations are reported in Table 1. Edge and curvature cues are only rely on lung boundary, therefore strong rib cage edges mislead the feature extraction algorithm. Curvature cue is mostly good at segmenting the bottom part of the lung because of the costophrenic angle curvature. However, it sometimes fails to segment the outer boundary of lung especially if the lung shape is not curved enough. On the other hand, the proposed approach combines edge, texture and curvature information in learning framework. Therefore, the segmentation with predicted  $\lambda$ -map produced better results than the single best  $\lambda$  and adaptive  $\lambda$  with other cues. Table 2 compares the segmentation results with predicted  $\lambda$ -map with the literature work.

Overlap Scores of Segmentation Masks				
$\lambda$ -map	Avg $\pm$ std	Min	Median	Max
$\lambda_G$ [20] <sup>1</sup>	0.857 $\pm$ 0.057	0.503	0.869	0.956
$\lambda_E$ [11]	0.831 $\pm$ 0.051	0.516	0.843	0.916
$\lambda_C$ [12]	0.831 $\pm$ 0.051	0.514	0.842	0.920
$\lambda_P$	0.901 $\pm$ 0.054	0.541	0.911	0.969
$\lambda_{GT}$	0.976 $\pm$ 0.024	0.732	0.938	0.994

**Table 1.** The overlap percentages between the ground truth segmentation and automated segmentation of all 247 images in lung database.

Method	Avg $\pm$ std	Min	Median	Max
<b>GC with <math>\lambda_{GT}</math></b>	<b>0.976 <math>\pm</math> 0.024</b>	<b>0.732</b>	<b>0.938</b>	<b>0.994</b>
Hybrid Voting [19]	0.949 $\pm$ 0.020	0.818	0.953	0.978
PC postprocessed [19]	0.945 $\pm$ 0.022	0.823	0.951	0.972
Hybrid ASM-PC [19]	0.934 $\pm$ 0.037	0.706	0.945	0.968
Hybrid AAM-PC [19]	0.933 $\pm$ 0.026	0.762	0.939	0.966
ASM-SIFT [21]	0.920 $\pm$ 0.031	0.783	0.928	0.961
ASM [19]	0.903 $\pm$ 0.057	0.601	0.924	0.960
<b>GC with <math>\lambda_P</math></b>	<b>0.901 <math>\pm</math> 0.054</b>	<b>0.541</b>	<b>0.911</b>	<b>0.969</b>
ASM [21]	0.870 $\pm$ 0.074	0.608	0.892	0.954
AAM [19]	0.847 $\pm$ 0.095	0.017	0.874	0.956
Mean shape [19]	0.713 $\pm$ 0.075	0.460	0.713	0.891

**Table 2.** Overlap scores on JSRT dataset compared to gold standard segmentation. GC: Graph Cut, PC: Pixel Classification, ASM: Active Shape Model, AAM: Active Appearance Model.

### 4. CONCLUSIONS AND FUTURE WORK

In this paper, we describe a methodology for adaptive parameter learning to improve the segmentation performance using

<sup>1</sup>Same scores as in [20] but calculated using overlap instead of Dice score.

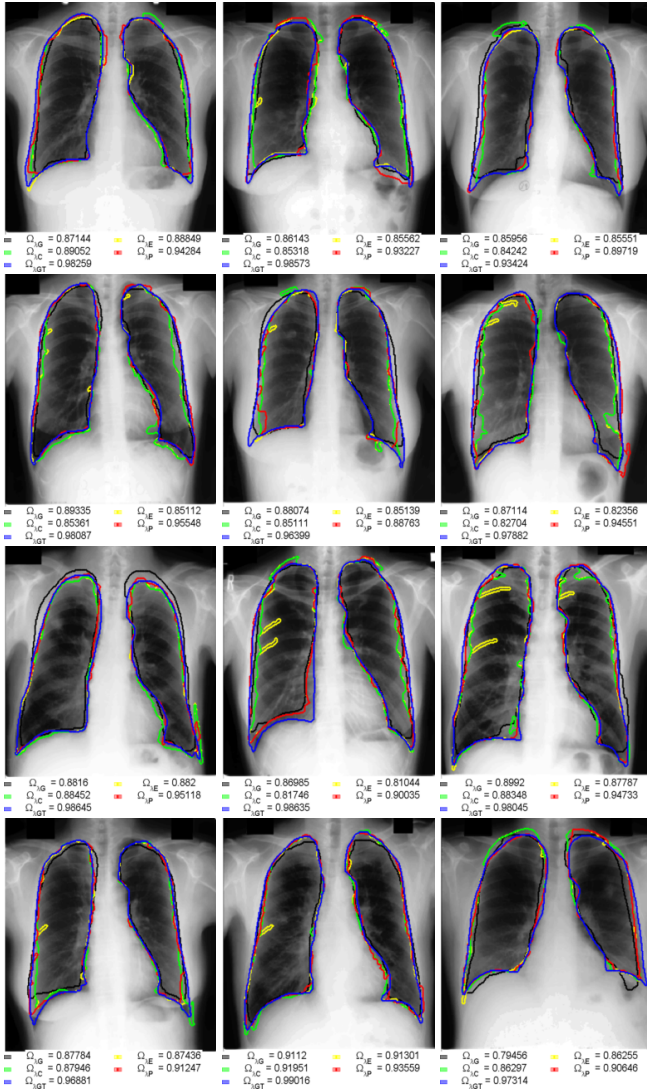


Fig. 4. Segmentations and their overlap scores

a multi-class classifier approach. We demonstrated the performance of the system within graph cut segmentation framework. The approaches in literature modulate the regularization parameter using a single feature or a heuristic combination of a few features. We model the characteristics of the image regions with feature vectors which includes haar feature for edge, local binary pattern for texture and hessian for shape information of local regions. Therefore our approach characterizes the image regions better than using single feature. The simple structure of the system allows to incorporate alternative features such as Scale Invariant Feature Transform which is one of the best performing feature descriptors among local descriptors [22]. In the experiments, we tested the proposed system on lung boundaries. JSRT set also contains clavicle and heart masks which are suitable to validate the system performance on other type of anatomical shapes. Future work

aims to segment other 2D and 3D anatomical shapes using stronger features and classifiers.

## 5. REFERENCES

- [1] B. Ginneken, B. Romeny, and M. Viergever, "Computer-aided diagnosis in chest radiography: A survey," *IEEE Trans. on Medical Imaging*, vol. 20, no. 12, pp. 1228–1241, 2001.
- [2] S. Jaeger, *et al.*, "Detecting tuberculosis in radiographs using combined lung masks," in *IEEE Eng. in Medicine and Biology Society*, 2012.
- [3] Y. Boykov and M.P. Jolly, "Interactive organ segmentation using graph cuts," *Medical Image Computing and Computer-Assisted Intervention*, pp. 276–286, 2000.
- [4] Y. Boykov and G. Funka-Lea, "Graph cuts and efficient n-d image segmentation," *Int. J. of Computer Vision*, vol. 70, pp. 109–131, 2006.
- [5] M. Bertero, T. A. Poggio, and V. Torre, "Ill-posed problems in early vision," *Technical Report, Massachusetts Institute of Technology*, 1988.
- [6] L. Zhang and S.M. Seitz, "Estimating optimal parameters for mrf stereo from a single image pair," *IEEE Trans. Pattern Anal. Mach. Intell.*, vol. 29, no. 2, pp. 331–342, 2007.
- [7] K. Krajssek and R. Mester, "Maximum likelihood estimator for choosing the regularization parameters in global optical flow methods," in *Int. Conf. on Image Processing*, 2006, pp. 1081–1084.
- [8] B. Peng and O. Veksler, "Parameter selection for graph cut based image segmentation," in *British Machine Vision Conference*, 2008.
- [9] J. Rao, *et al.*, "Adaptive contextual energy parameterization for automated image segmentation," in *Int. Symp. on Visual Computing*, 2009.
- [10] G. Gilboa, *et al.*, "Nonlocal convex functionals for image regularization," *UCLA CAM-report*, 2006.
- [11] S. Candemir and Y. S. Akgul, "Adaptive regularization parameter for graph cut segmentation," in *Int. Conf. on Image Analysis and Recognition*, 2010, vol. 1, pp. 117–126.
- [12] J. Rao, *et al.*, "Adaptive regularization for image segmentation using local image curvature cues," in *European Conf. on Computer Vision*, 2010, pp. 651–665.
- [13] J. Friedman, T. Hastie, and R. Tibshirani, "Additive logistic regression: A statistical view of boosting," *Technical Report*, 1998.
- [14] J. Shiraishi, *et al.*, "Development of a digital image database for chest radiographs with and without a lung nodule: receiver operating characteristic analysis of radiologists' detection of pulmonary nodules," *American Journal of Roentgenology*, vol. 174, pp. 71–74, 2000.
- [15] C. Papageorgiou, M. Oren, and T. Poggio, "A general framework for object detection," in *Int. Conf. on Computer Vision*, 1998.
- [16] P. Viola and M. Jones, "Rapid object detection using boosted cascade of simple features," in *Computer Vision and Pattern Recognition*, 2001.
- [17] T. Ojala, M. Pietikainen, and T. Maenpaa, "Multiresolution grayscale and rotation invariant texture classification with local binary patterns," *IEEE Trans. Pattern Anal. Mach. Intell.*, pp. 971–987, 2002.
- [18] A. Frangi, *et al.*, "Multiscale vessel enhancement filtering," in *Medical Image Computing and Computer-Assisted Intervention*, pp. 130–137, 1998.
- [19] B. Ginneken, *et al.*, "Segmentation of anatomical structures in chest radiographs using supervised methods: a comparative study on a public database," *Medical Image Analysis*, vol. 10, no. 1, pp. 19–40, 2006.
- [20] S. Candemir, *et al.*, "Graph-cut based automatic lung boundary detection in chest radiographs," in *IEEE Healthcare Technology Conference: Translational Engineering in Health & Medicine*, 2012, pp. 31–34.
- [21] Y. Shi, *et al.*, "Segmenting lung fields in serial chest radiographs using both population-based and patient-specific shape statistics," *IEEE Trans. Medical Imaging*, vol. 27, no. 4, 2008.
- [22] K. Mikolajczyk and C. Schmid, "A performance evaluation of local descriptors," *IEEE Trans. Pattern Anal. Mach. Intell.*, vol. 27, no. 10, pp. 1615–1630, 2005.